

Large-scale *ab initio* simulations for periodic system

Xuecheng Shao^{a,b}, Qiang Xu^{a,b}, Sheng Wang^{a,b}, Jian Lv^{a,b,c}, Yanchao Wang^{a,b,*}, Yanming Ma^{a,b,*}

^a State Key Laboratory of Superhard Materials, College of Physics, Jilin University, Changchun 130012, China

^b Innovation center of computational physics methods and software, College of Physics, Jilin University, China

^c College of Materials Science and Engineering, Jilin University, Changchun 130012, China

ARTICLE INFO

Article history:

Received 24 November 2017

Received in revised form 29 June 2018

Accepted 12 July 2018

Available online 20 July 2018

Keywords:

OF-DFT

Molecular dynamics

Parallel

ATLAS

ABSTRACT

In this manuscript, we present new capabilities and implementations on massively parallel computers of our *ab initio* orbital-free density functional theory software (ATLAS). In addition to the electronic ground-state capabilities, the extensive structure-related functionalities including geometrical structure relaxation and molecular dynamics simulation have been implemented in the new version of ATLAS. The effectiveness of these extensions is assessed through simulations of nanocrystalline and warm dense Al. The simulated results agree excellently with previous experimental and theoretical data, validating new capabilities. Furthermore, new version of ATLAS exploiting the massively parallel implementation with message passing interface shows high efficiency, as exemplified by its ability to simulate a system containing 4 million atoms only taking less than 1 h with 2048 processors. The scalable parallel implementation of the ATLAS package with extensive capabilities holds considerable promise for simulation of large-scale systems with millions of atoms.

© 2018 Elsevier B.V. All rights reserved.

1. Introduction

The *ab initio* method based on the traditional Kohn–Sham density functional theory (KS-DFT) [1,2] has become an invaluable tool across a wide range of disciplines, including materials physics and chemistry, earth sciences, surface science, and biology [3–7] because of its accurate descriptions of materials' properties. However, KS-DFT approaches have long been considered inappropriate for simulating systems of ten thousands of atoms because of their heavy computational demands, which scale as $O(N^3)$, where N is the total number of electrons [8–10]. The development of a new approach to accelerate these calculations without greatly sacrificing accuracy is thus highly desirable. Orbital-free density functional theory (OF-DFT) is potentially an efficient theory for large-scale quantum mechanical simulations because of its linear scaling behavior [10,11].

Recently, we developed a real-space finite-difference method for the numerical solution of OF-DFT using a direct energy-minimization scheme for periodic systems and coded it into the ATLAS software package [11,12]. The accuracy of our method is demonstrated through direct comparisons to results from KS-DFT simulations for periodic systems of Mg, Al, and Al_3Mg . Particularly, our calculations indicate that our method can be used to simulate systems containing ten thousands of atoms per cell using a single

processor. However, the capability of only static calculations of the total energy in this ATLAS package severely limits its applicability, as the package cannot be used to simulate the atomistic processes of real systems. In particular, our previous ATLAS package only implemented a sequential scheme, impeding its application for simulations of large-scale systems. Extension of the capabilities and implementation of a parallel scheme of ATLAS are crucial to its future success and popularity.

This work provides an overview of the latest ATLAS developments, focusing primarily on extensive capabilities including geometrical structure relaxation and molecular dynamics (MD) modules (Fig. 1(a)). In particular, a massively parallel scheme was implemented in a new version of the ATLAS package to accelerate significantly the simulation rate by utilizing large-scale parallel computers. The remainder of the text is organized as follows. Section 2 presents the detailed implementation of geometrical structure relaxation, MD, and parallelism of the ATLAS package. We evaluate the numerical performance of ATLAS for a periodic solid Al system and warm dense matter (WDM) in Section 3. Finally, concluding remarks are presented in Section 4.

2. Theory and background

2.1. Geometrical structure relaxation

One major application of theoretical simulations is geometrical structure relaxation; i.e., determination of a local minimum on the

* Corresponding authors.

E-mail addresses: wyc@calypso.cn (Y. Wang), mym@jlu.edu.cn (Y. Ma).

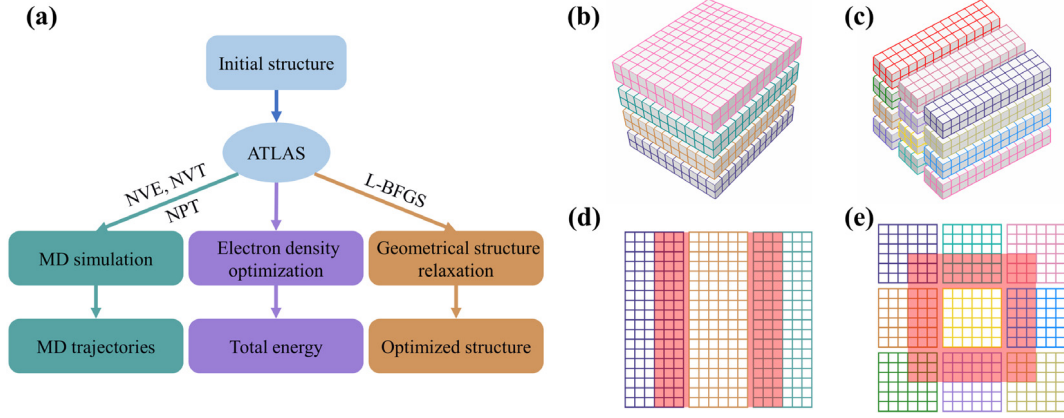


Fig. 1. (a) Capabilities of ATLAS. (b) Slab domain decomposition using four processors. (c) Pencil domain decomposition using a 4×3 processor grid. The buffer region (reddish) is used to store information for the points near a domain boundary for the center processor in slab (d) and pencil (e) decompositions. (For interpretation of the references to color in this figure legend, the reader is referred to the web version of this article.)

potential energy surface and the corresponding atomic configuration for a given initial configuration. Geometry relaxation finds a physically significant structure of a substance associating with a substance as it is found in nature, which can then be used in various theoretical investigations. The process aims to determine the atomic configuration with minimized energy, for which the force on each atom is acceptably close to zero.

The success of geometry relaxation depends on the accuracy of the calculated forces. The forces on nuclei consists of vectors of negative derivatives of the total energy with respect to the nuclear coordinates. According to OF-DFT, the total energy functional $E[\rho(\mathbf{r})]$ of a N-electron system can be written (in atomic units) as follows [13,14]:

$$E[\rho(\mathbf{r})] = T[\rho(\mathbf{r})] + E_H[\rho(\mathbf{r})] + E_{XC}[\rho(\mathbf{r})] + E_{I-E} + E_{I-I}, \quad (1)$$

where $T[\rho(\mathbf{r})]$, $E_H[\rho(\mathbf{r})]$, $E_{XC}[\rho(\mathbf{r})]$, E_{I-E} and E_{I-I} represent the electronic kinetic energy, Hartree electron–electron repulsion energy, exchange–correlation energy, electron–ion interaction energy, and ion–ion repulsion energy, respectively. The force on each ion under periodic boundary conditions is calculated as follows:

$$\mathbf{F}_j = \frac{-\partial E[\rho]}{\partial \mathbf{R}_j} = \mathbf{F}_{I-E,j} + \mathbf{F}_{I-I,j}, \quad (2)$$

where \mathbf{R}_j is the position of the j th ion. The force on each ion is clearly related to only the ion–electron and ion–ion interactions. The force $F_{I-E,j}$ can be expressed as

$$\mathbf{F}_{I-E,j\in\alpha} = 2\Omega \sum_{\mathbf{g}>0} \mathbf{g} v_{loc}^\alpha(|\mathbf{g}|) \text{Im}[\rho(\mathbf{g}) e^{i\mathbf{g}\cdot\mathbf{R}_j}], \quad (3)$$

where Ω is the volume of the unit cell; \mathbf{g} is determined by the primitive vectors of reciprocal space; $v_{loc}^\alpha(|\mathbf{g}|)$ and $\rho(\mathbf{g})$ denote the ionic pseudopotential of the α th atomic species and the Fourier components of the electron density, respectively. Obviously, it is limited to relatively small systems due to cubic-scaling behavior for Eq. (3). Thus, a powerful linear scaling method with the cardinal B-spline particle mesh Ewald [10] was employed to evaluate the contribution of potential and forces for ion–electron interactions.

Finally, the force of ion–ion contribution [15,16] can be calculated using

$$\mathbf{F}_{I-I,j} = \mathbf{F}_{I-I,j}^{dir} + \mathbf{F}_{I-I,j}^{rec}, \quad (4)$$

Here,

$$\mathbf{F}_{I-I,j}^{dir} = \frac{\partial E^{dir}}{\partial \mathbf{R}_j} = \frac{q_j}{\beta^3} \sum_{k=1, k \neq j}^M \sum_n q_k (\mathbf{R}_j - \mathbf{R}_k + \mathbf{n})$$

$$\times \left[\frac{\text{erfc}(\beta R_{jk,n})}{(\beta R_{jk,n})^3} + \frac{2}{\sqrt{\pi}} \frac{e^{-(\beta R_{jk,n})^2}}{(\beta R_{jk,n})^2} \right] \quad (5)$$

and

$$\mathbf{F}_{I-I,j}^{rec} = \frac{4\pi}{\Omega} q_j \sum_{\mathbf{g} \neq 0} \mathbf{g} \left[\sin(\mathbf{g} \cdot \mathbf{R}_j) \sum_k q_k \cos(\mathbf{g} \cdot \mathbf{R}_k) - \cos(\mathbf{g} \cdot \mathbf{R}_j) \sum_k q_k \sin(\mathbf{g} \cdot \mathbf{R}_k) \right] \frac{e^{-(|\mathbf{g}|/2\beta)^2}}{|\mathbf{g}|^2}. \quad (6)$$

Here, β is a parameter that controls the convergence rates of the direct and reciprocal Ewald sums, q_j is the charge on the j th ion, M is the number of ions in the unit cell, \mathbf{n} is the lattice vector of periodic cell images, $\text{erfc}(x)$ is the complementary error function, and $R_{jk,n} = |\mathbf{R}_j - \mathbf{R}_k + \mathbf{n}|$. As the computational cost of calculating the force of the ion–ion contribution for standard Ewald summation scales quadratically, the particle–mesh Ewald method [17,18] with linear scaling was employed to calculate the ion–ion energy and corresponding force in our ATLAS package.

Currently, various well-established local optimization algorithms (e.g., steepest descent, conjugate gradient, quasi-Newton, and Fast Inertial Relaxation Engine) [19,20] are available. Compared with the traditional conjugate gradient, the Broyden–Fletcher–Goldfarb–Shanno (BFGS) method [21], the most popular quasi-Newton algorithm, is widely applied to geometry relaxation because of its fast convergence rate. However, it is infeasible to optimize the case associated with a large number of variables because of the large memory storage requirements. An improved limited-memory quasi-Newton method (L-BFGS) [22] only requires limited computer memory, and is thus particularly suitable for complex optimization problems. Therefore, we implemented the L-BFGS method in our ATLAS package to perform geometry relaxation.

2.2. Molecular dynamics

MD simulation is widely used in materials science and chemistry. MD simulations under experimental conditions enable experimental activity to be viewed as it occurs, and can provide information that is not directly attainable from experiments to help understand empirical observations. The reliability of MD simulations has always been limited by three factors: (i) the accuracy of the forces acting on the nuclei in each MD simulation step, (ii) the computational system size, and (iii) the length of the simulation [23]. Although traditional *ab initio* MD simulations in the framework of KS-DFT can provide accurate forces, they are limited

to relatively small system sizes and time scales. Thus, traditional ab initio MD is inappropriate for modeling many atomistic processes, where realism can only be achieved by simulating a large system (millions of atoms) for a long time (nanoseconds) [23]. Notably, the computational costs of calculating forces in the framework of OF-DFT scale linearly, which allows access to length scales directly relevant to experimental studies. In principle, sub-micrometer lengths can be accessed in nanoseconds with available computer resources.

The microcanonical (NVE), canonical (NVT), and isothermal-isobaric (NPT) ensembles are the three most widely used ensembles for MD simulations, and they all have been implemented into our ATLAS package. The NVE ensemble can be used to model isolated systems of interest, where the classical equations of motion are adopted to describe particle motion. The NVT ensemble allows effective control of the temperature using the Nosé–Hoover thermostat [24,25]. For this ensemble, the following equations of motion for particles are used:

$$\begin{aligned} \dot{\mathbf{r}}_j &= \frac{\mathbf{p}_j}{m_j}, & \dot{\mathbf{p}}_j &= \mathbf{F}_j - \frac{p_\eta}{Q} \mathbf{p}, \\ \dot{\eta} &= \frac{p_\eta}{Q}, & \dot{p}_\eta &= \sum_j \frac{\mathbf{p}_j^2}{m_j} - N_f k_B T, \end{aligned} \quad (7)$$

where \mathbf{r}_j is the position of the j th ion with mass m_j , and η is the thermostat with effective mass Q and momentum p_η . The NPT ensemble can be used to simulate systems with constant temperature and pressure. Specifically, the temperature is also controlled using the Nosé–Hoover thermostat, and the pressure is adjusted using two typical barostat approaches developed by Andersen [26] and Parrinello–Rahman [27]. In the former method, the pressure associated with isotropic fluctuations of the simulation cell only depends on a single variable of volume, whereas in the latter, the pressure is controlled by variations of the volume and shape of the simulation cell.

2.3. Parallel implementation

Our previous studies have illustrated the use of ATLAS with the sequential scheme as a powerful tool for a single processor to simulate a system containing ten thousands of atoms in a simulated cell [12]. However, it remains a great challenge to simulate large systems containing millions of atoms without parallelism. Thus, it is highly desirable to implement a parallel scheme for ATLAS to take full advantage of the massive parallelism available on modern high-performance computing architectures for large-scale simulations. A real-space finite difference expansion [28] involving short-range operations was employed in our ATLAS method. An efficient implementation of this method on parallel computers is thus expected to be possible because it minimizes the amount of data that must be communicated between processors.

In our parallelization scheme, all the terms of the Hamiltonian on the real-space grids were implemented on massively parallel computers based on spatial decomposition, in which the 3D domain was divided into equal-sized blocks with each block being assigned to a processor in a parallel computer. Currently, two decomposition schemes, slab (1D) and pencil (2D) decomposition, have been employed to divide the real-space grid points in our approach. As illustrated in Fig. 1(b) and (c), the blocks are distributed along only one axis in slab decomposition, whereas the 3D domain can be partitioned into two dimensions in pencil decomposition. The message passing interface is employed to handle data communication in ATLAS. As illustrated in Fig. 1(d) and (e), an additional buffer region was created to store information for the points near a domain boundary, which is used to perform finite difference schemes for each processor. Thus, the calculation can be run in

each processor for each domain, significantly improving system performance by reducing the communication frequency. Consequently, there is no need for the massive communication required in whole iterations except for the fast Fourier transform (FFT). Therefore, the calculated efficiency of ATLAS is mainly determined by the performance of the FFT. In our ATLAS package, the parallel FFT libraries with the slab (FFTW) [29] and pencil (2DECOMP&FFT) decompositions [30] were used to achieve high efficiency with optimal memory use.

3. Numerical results

To illustrate the new capabilities of ATLAS, structure relaxation of a nanocrystalline structure of Al and MD simulations of warm dense Al were performed. Calculations employed the local density approximation exchange–correlation functional with Perdew–Zunger parameterization [31]. The Wang–Teter [32] and finite-temperature Thomas–Fermi approaches [33] were used for the kinetic energy density functional for the geometrical structure relaxation and MD simulations, respectively. The optimized effective pseudopotential [34] scheme was used to construct the local pseudopotential of Al, with valence electronic configuration of $3s^2 3p^1$ and core cutoff radius of 1.2 Å. A system grid spacing of 0.2 Å and sixth-order finite-difference expansion were used to ensure that the total energy calculations converged to less than 1 meV/atom. All the parallelized calculations were performed using the high-performance Tianhe-1A supercomputer at the National Supercomputer Center of Tianjin, where each node contains a 6-core/12-thread Xeon X5650 CPU with 24-GB memory with a maximum interconnect speed of 160 GBps.

To test the convergence of the geometrical structure relaxation of ATLAS for a large system, a nanocrystalline structure containing 181,440 Al atoms in a cubic cell was selected as a benchmark. For this system, a length of 150 Å can be achieved for the simulated cell, with the corresponding grid size in real space reaching $768 \times 768 \times 768$. The total energy and maximum force as a function of the number of L-BFGS steps during the geometry optimization are presented in Fig. 2(a) and (b), respectively. Specifically, it only takes approximately 100 steps for the total energy to converge to within 1 meV/atom, whereas the maximal force is less than 0.02 eV/Å until 669 L-BFGS iterations (729 force estimations). Given the complex structure is employed as initial structure in our calculation, ATLAS yields significantly faster convergence.

Notably, the force convergences more slowly than the total energy. Acceleration of the convergence rate of the force is critical for geometry relaxation of large-scale systems. Recently, Chen et al. proposed a new curved-line search algorithm, which can speed up ab initio atomic structure relaxation by a factor of 2–4 with respect to traditional methods [35]. Thus, this new curved-line search algorithm will be implemented to speed up the force convergence of ATLAS in the future.

WDM belongs to either equilibrium or non-equilibrium states of matter, which is characterized by elevated temperature (up to 100 eV) and high pressures (up to hundreds of TPa). Because of the large abundance in the interiors of some large planets [36,37], in-depth investigations of WDM is critical to understand better the physics and chemistry of these planetary interiors. However, the creation and investigation of WDM under controlled conditions in the laboratory is difficult, MD simulation becomes an alternative approach. It is generally accepted that the required number of orbitals scales with temperature in KS-DFT. These calculations therefore become computationally expensive at elevated temperature because of the large number of fractionally occupied KS orbitals that must be considered. In contrast, the OF-DFT method only depends on the density without suffering from scaling issues. Thus, by offering accessibility to ultra-high temperatures at low computational cost, the OF-DFT method is an invaluable tool to model

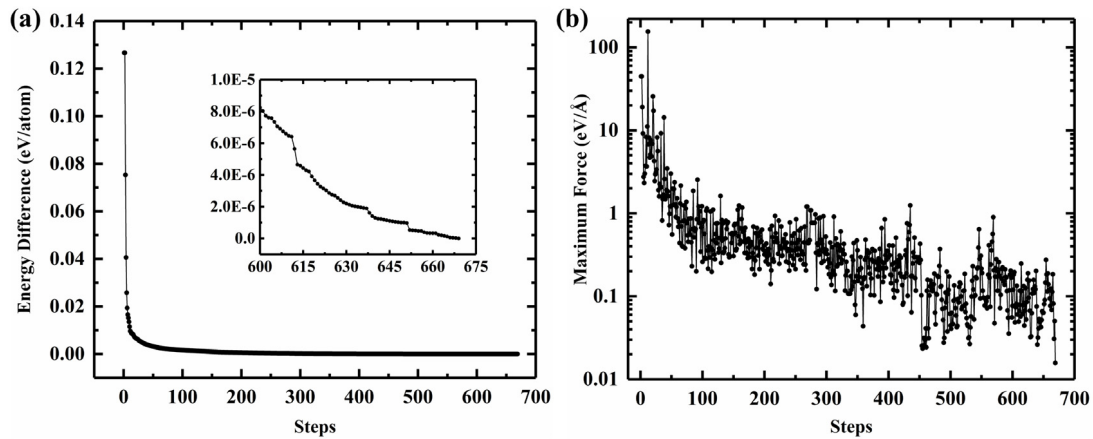


Fig. 2. Evolution of total energy (a) and maximum force (b) as functions of the number of L-BFGS steps during geometry relaxation for a nanocrystalline structure. The inset of (a) shows the evolution of the total energy for the last few dozen steps.

WDM. Furthermore, previous studies have shown that the finite-temperature Thomas–Fermi kinetic energy density functional is suitable to simulate WDM with sufficient precision [33,38]. Therefore, simulations of warm dense Al were performed to test the applicability of ATLAS for first-principles MD simulations.

Our MD simulations were performed using a supercell containing 500 atoms with the NVT ensemble, and the Nosé–Hoover thermostat was used to control the temperature. Long-timescale molecular dynamic simulations are required to obtain reliable statistical results, and the time step must be small enough to sample accurately the highest frequency motion for simulation at high temperature. A time step of 0.25 fs and a total simulation time of 25 ps (100,000 steps) were employed in our simulation. The system was initially equilibrated for 5000 MD steps, and data were collected from the subsequent 95,000 steps.

The wavenumber-resolved scattering data $W(k)$ representing the ion character of Al were calculated using ATLAS in warm dense regimes, where the density and temperature of the sample are (6.3 g/cm³, 1.75 eV) and (8.1 g/cm³, 10 eV), respectively. The calculated data are compared with experimental data [39,40] and previous theoretical data [40,41] in Fig. 3. Our simulated results at 6.3 g/cm³ and 1.75 eV are in excellent agreement with the experimental data [40], which further confirms the reliability of the MD simulation in ATLAS (Fig. 3(a)). However, the theoretical data obtained using our OF-DFT and previous KS-DFT simulations [39] at 8.1 g/cm³ and 10 eV do not agree with the experimental measurement. Specifically, the calculated height of the high-intensity peak was significantly underestimated compared with that for the experimental data. One possible reason provided by previous studies [42,43] is that the system is associated with non-equilibrium states, where the ionic temperature (T_i) is lower than the experimentally measured electronic temperature (T_e). To estimate the experimental T_i , non-equilibrium MD simulations were performed using our ATLAS package at different values of T_i with a constant T_e of 10 eV. The calculated wavenumber-resolved scattering data are compared with experimental data in Fig. 3(b). The simulated data for $T_i = 2$ eV agree well with the experiment data. Thus, our results support the deduction of a non-equilibrium state existing for the experimental measurement with $T_e = 10$ eV and $T_i = 2$ eV.

To evaluate the performance of slab and pencil decompositions, the static total energy of Al with a supercell fcc structure containing 32,000 atoms was calculated using the ATLAS package. Fig. 4(a) compares the wall time calculated using the two spatial decompositions. Our results demonstrate that the performances of the two approaches were comparable for less than 200 processors. However, for more than 200 processors, the pencil decomposition significantly outperformed the slab spatial decomposition. It

should be emphasized that the maximum achievable theoretical limit of the spatial decomposition scheme can be estimated from the maximized number of divided blocks, because each block is assigned to a processor. For the system, which is discretized to a mesh of $n_r = n_x \times n_y \times n_z$ spatial collocation points, the maximized number of divided blocks is determined by $\max(n_x, n_y, n_z)$ and $n_r/\min(n_x, n_y, n_z)$ for the slab and pencil decomposition algorithms, respectively. It is reasonably understood that pencil decomposition is generally more efficient than slab decomposition on a large number of processors. Therefore, the pencil decomposition was employed in the following massively parallel calculations.

To illustrate the computation time for each term, we perform a full optimization of a system containing 1.372 million Al atoms using 2048 processors. The time spent calculating each of terms (summing all the time contributions of energy, potential, stress and force) are presented in Fig. 4(b). The kinetic terms of Thomas–Fermi (TF) and von Weizsäcker (VW), and exchange–correlation term are evaluated in real space, while the Hartree and the nonlocal part of Wang–Teter (WT) functional are mainly calculated in reciprocal space using FFT. All the terms calculated in real-space are approximately linear scaling as the number of atoms is increased, while the dominant contribution comes from evaluation of the terms including nonlocal part of WT (45%) and Hartree (20%) due to involving the large number of FFTs. Furthermore, these terms can also be calculated using real-space method with the large scaling of the parallelization, we will try to use the real-space method for further optimization.

To evaluate the computational efficiency of the parallel ATLAS package, static simulations of a supercell structure of Al containing different numbers of atoms was performed using 2048 processors. The total wall time and its contributions for optimizing the electron density and evaluating the force and stress as a function of the number of atoms are presented in Fig. 5(a). The total wall time for simulating a large system containing 4 million atoms was only less than 1 h, indicating the high efficiency of ATLAS. It is noteworthy that the parallel ATLAS package retains approximately linear time scaling for sizes up to 4 million atoms and that the time for evaluating the force and stress is negligible. To illustrate the parallel scalability of ATLAS, we performed a static simulation of a fcc Al periodic supercell containing 2.048 million atoms using different processors. The speedup ratio and parallel efficiency as a function of the number of processors with respect to 1024 processors are plotted in Fig. 5(b). The parallel efficiency reached 0.920 for 2.048 million atoms on 4096 processors, demonstrating the strong parallel scaling of ATLAS for simulations of large-scale systems.

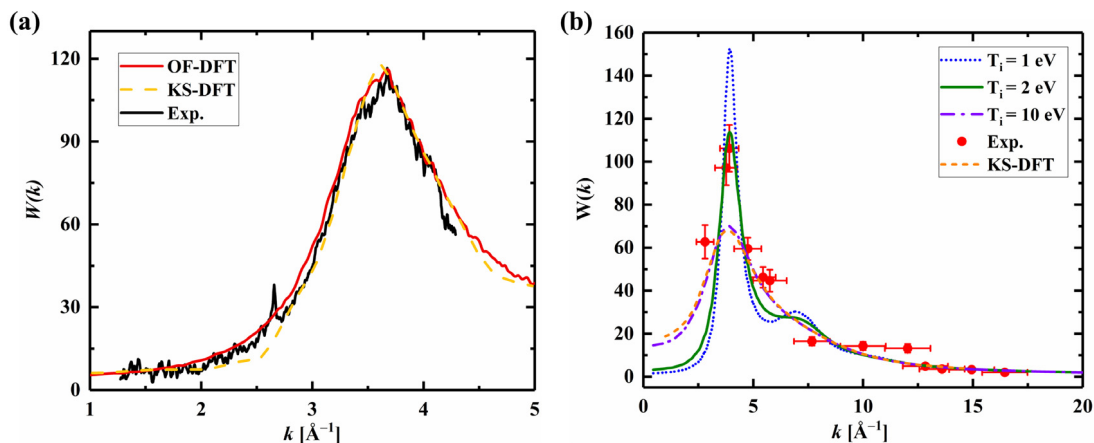


Fig. 3. (a) Wavenumber-resolved scattering data of Al calculated at 6.3 g/cm^3 and 1.75 eV with ATLAS compared with experimental and previous KS-DFT data. (b) Our calculated wavenumber-resolved scattering data with $T_i = 1, 2,$ and 10 eV and $T_e = 10 \text{ eV}$. To facilitate the comparison, experimental and previous theoretical data are also shown.

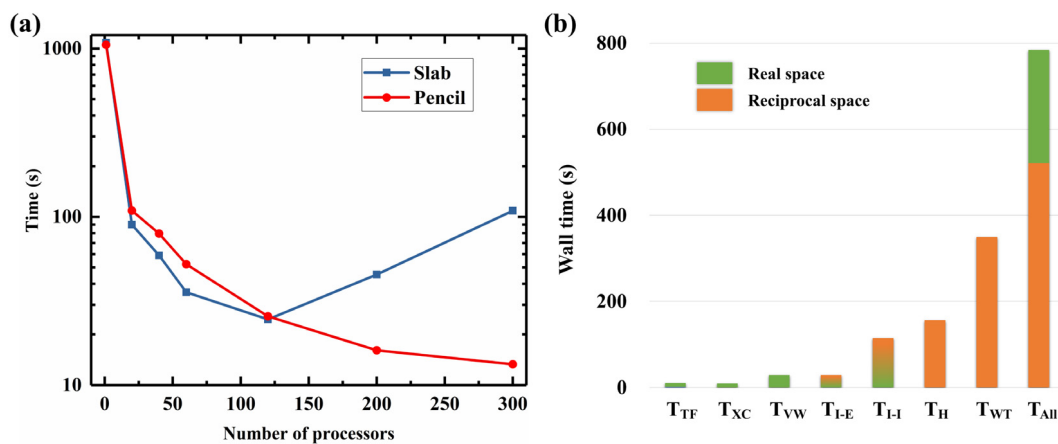


Fig. 4. (a) Comparison of total time (wall time) for density optimization of Al with a supercell fcc structure containing 32,000 atoms with slab and pencil domain decompositions. (b) The time spent on each of the terms during the optimization for a system containing 1.372 million Al atoms using 2048 processors with ATLAS. T_{All} is the total time.

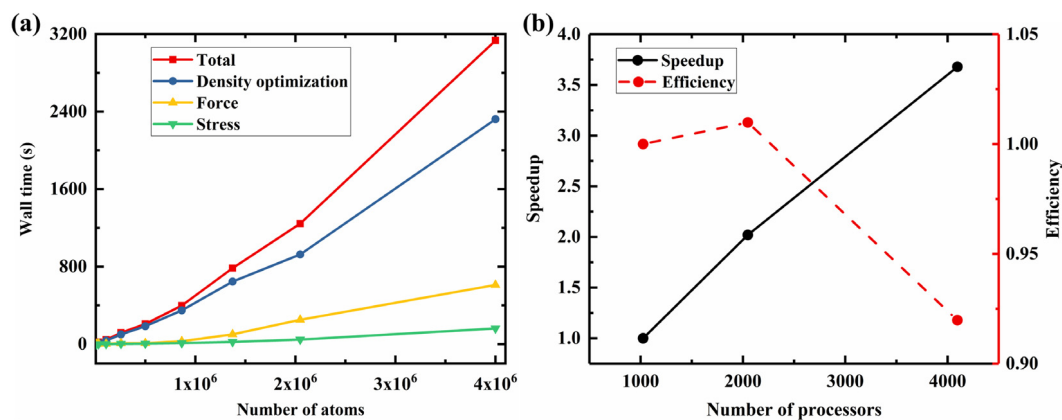


Fig. 5. (a) Total time (wall time) using ATLAS to perform a static calculation including density optimization, force and stress estimation for an Al supercell containing up to 4 million atoms using 2048 processors. (b) Speedup ratio (solid line) and parallel efficiency (dash line) as a function of the number of processors.

4. Conclusion

In this article, we have presented the extensions of structure-related capabilities of ATLAS including atomic structure relaxation and finite temperature molecular dynamics simulations. The extended capabilities have been validated by the simulations of

periodic metallic Al. Moreover, the parallel version of ATLAS was developed to effectively take full advantage of the massive parallelism. The simulations indicate that the new version of ATLAS has high efficiency and strong scalability, making it as a highly efficient and portable massively parallel computational tool for a wide range of materials science issues of large-scale systems.

Acknowledgments

The authors acknowledge the funding support from the National Key Research and Development Program of China under Grant No. 2016YFB0201200, 2016YFB0201201, 2017YFB0701503 the National Natural Science Foundation of China (Grant Nos. 11774127, 11404128 and 11534003), and the Science Challenge Project No. TZ2016001. Parts of the calculations were performed at the High-Performance Computing Center of Jilin University and Tianhe2-JK in the Beijing Computational Science Research Center.

References

- [1] W. Kohn, L.J. Sham, *Phys. Rev.* 140 (1965).
- [2] P. Hohenberg, W. Kohn, *Phys. Rev.* 136 (1964) B864–B871.
- [3] Y. Ma, M. Eremets, A.R. Oganov, Y. Xie, I. Trojan, S. Medvedev, A.O. Lyakhov, M. Valle, V. Prakapenka, *Nature* 458 (2009) 182–185.
- [4] J. Lv, Y. Wang, L. Zhu, Y. Ma, *Phys. Rev. Lett.* 106 (2011) 015503.
- [5] L. Zhu, H. Liu, C.J. Pickard, G. Zou, Y. Ma, *Nature Chem.* 6 (2014) 644–648.
- [6] S. Lu, Y. Wang, H. Liu, M. Miao, Y. Ma, *Nature Commun.* 5 (2014) 1–6.
- [7] R. Iftimie, P. Minary, M.E. Tuckerman, *Proc. Natl. Acad. Sci. USA* 102 (2005) 6654–6659.
- [8] M.C. Payne, M.P. Teter, D.C. Allan, T.A. Arias, J.D. Joannopoulos, *Rev. Modern Phys.* 64 (1992) 1045–1097.
- [9] E.A. Carter, *Science* (80-.) 321 (2008) 800–803.
- [10] L. Hung, E.A. Carter, *Chem. Phys. Lett.* 475 (2009) 163–170.
- [11] W. Mi, X. Shao, C. Su, Y. Zhou, S. Zhang, Q. Li, H. Wang, L. Zhang, M. Miao, Y. Wang, Y. Ma, *Comput. Phys. Comm.* 200 (2016) 87–95.
- [12] X. Shao, W. Mi, Q. Xu, Y. Wang, Y. Ma, *J. Chem. Phys.* 145 (2016) 1–5.
- [13] Y.A. Wang, E.A. Carter, in: S.D. Schwartz (Ed.), *Theor. Methods Condens. Phase Chem.*, Kluwer Academic Publishers, Dordrecht, 2002, pp. 117–184.
- [14] V.V. Karasiev, S.B. Trickey, *Comput. Phys. Comm.* 183 (2012) 2519–2527.
- [15] P.P. Ewald, *Ann. Phys.* 369 (1921) 253–287.
- [16] N. Karasawa, W.A. Goddard, *J. Phys. Chem.* 93 (1989) 7320–7327.
- [17] T. Darden, D. York, L. Pedersen, *J. Chem. Phys.* 98 (1993) 10089–10092.
- [18] U. Essmann, L. Perera, M.L. Berkowitz, T. Darden, H. Lee, L.G. Pedersen, *J. Chem. Phys.* 103 (1995) 8577–8593.
- [19] J. Nocedal, S.J. Wright, *Numerical Optimization*, Springer-Verlag, New York, 1999.
- [20] E. Bitzek, P. Koskinen, F. Gähler, M. Moseler, P. Gumbsch, *Phys. Rev. Lett.* 97 (2006) 170201.
- [21] R. Fletcher, *Practical Methods of Optimization*, second ed., Wiley-Interscience, New York, NY, USA, 1987.
- [22] D.C. Liu, J. Nocedal, *Math. Program.* 45 (1989) 503–528.
- [23] S.J. Zhou, D.M. Beazley, *Science* (80-.) 3 (1996) 183–186.
- [24] S. Nosé, *J. Chem. Phys.* 81 (1984) 511–519.
- [25] W.G. Hoover, *Phys. Rev. A* 31 (1985) 1695–1697.
- [26] H.C. Andersen, *J. Chem. Phys.* 72 (1980) 2384–2393.
- [27] M. Parrinello, A. Rahman, *J. Appl. Phys.* 52 (1981) 7182–7190.
- [28] K. Hirose, T. Ono, Y. Fujimoto, S. Tsukamoto, *First-Principles Calculations in Real-Space Formalism - Electronic Configurations and Transport Properties of Nanostructures*, Imperial College Press, 2005.
- [29] M. Frigo, S.G. Johnson, *Proc. 1998 IEEE Int. Conf. Acoust. Speech Signal Process., ICASSP '98 (Cat. 98CH36181)*, IEEE, 1998, pp. 1381–1384.
- [30] N. Li, S. Laizet, *Cray User Gr. 2010 Conf. 2010*, pp. 1–13.
- [31] J.P. Perdew, A. Zunger, *Phys. Rev. B* 23 (1981) 5048–5079.
- [32] L.W. Wang, M.P. Teter, *Phys. Rev. B* 45 (1992) 13196–13220.
- [33] V.V. Karasiev, T. Sjoström, S.B. Trickey, *Phys. Rev. B* 86 (2012) 115101.
- [34] W. Mi, S. Zhang, Y. Wang, Y. Ma, M. Miao, *J. Chem. Phys.* 144 (2016).
- [35] Z. Chen, J. Li, S. Li, L.-W. Wang, *Phys. Rev. B* 96 (2017) 115141.
- [36] T. Guillot, *Science* (80-.) 286 (1999) 72–77.
- [37] J. Daligault, S. Gupta, *Astrophys. J.* 703 (2009) 994–1011.
- [38] J. Clérouin, G. Robert, P. Arnault, C. Ticknor, J.D. Kress, L.A. Collins, *Phys. Rev. E: Stat. Nonlinear Soft Matter Phys.* 91 (2015) 1–5.
- [39] T. Ma, T. Döppner, R.W. Falcone, L. Fletcher, C. Fortmann, D.O. Gericke, O.L. Landen, H.J. Lee, A. Pak, J. Vorberger, K. Wünsch, S.H. Glenzer, *Phys. Rev. Lett.* 110 (2013) 065001.
- [40] L.B. Fletcher, H.J. Lee, T. Döppner, E. Galtier, B. Nagler, P. Heimann, C. Fortmann, S. LePape, T. Ma, M. Millot, A. Pak, D. Turnbull, D.A. Chapman, D.O. Gericke, J. Vorberger, T. White, G. Gregori, M. Wei, B. Barbrel, R.W. Falcone, C.-C. Kao, H. Nuhn, J. Welch, U. Zastra, P. Neumayer, J.B. Hastings, S.H. Glenzer, *Nat. Photonics* 9 (2015) 274–279.
- [41] H.R. Rüter, R. Redmer, *Phys. Rev. Lett.* 112 (2014) 145007.
- [42] J. Clérouin, G. Robert, P. Arnault, C. Ticknor, J.D. Kress, L.A. Collins, *Phys. Rev. E* 91 (2015) 011101.
- [43] C.E. Starrett, D. Saumon, *Phys. Rev. E* 92 (2015) 033101.